HHS Public Access

Author manuscript

Thin Solid Films. Author manuscript; available in PMC 2017 January 01.

Published in final edited form as:

Thin Solid Films. 2016 January 1; 598: 16–24. doi:10.1016/j.tsf.2015.11.082.

Nanoparticle layer deposition for highly controlled multilayer formation based on high- coverage monolayers of nanoparticles

Yue Liu[1,#], **Mackenzie G. Williams**[1,#], **Timothy J. Miller**[1,#], and **Andrew V. Teplyakov**[1,*]

[1]Department of Chemistry and Biochemistry, University of Delaware, Newark, DE 19716, USA

Abstract

This paper establishes a strategy for chemical deposition of functionalized nanoparticles onto solid substrates in a layer-by-layer process based on self-limiting surface chemical reactions leading to *complete* monolayer formation within the multilayer system without any additional intermediate layers – nanoparticle layer deposition (NPLD). This approach is fundamentally different from previously established traditional layer-by-layer deposition techniques and is conceptually more similar to well-known atomic and molecular – layer deposition processes. The NPLD approach uses efficient chemical functionalization of the solid substrate material and complementary functionalization of nanoparticles to produce a nearly *100% coverage* of these nanoparticles with the use of “click chemistry”. Following this initial deposition, a second *complete monolayer* of nanoparticles is deposited using a copper-catalyzed “click reaction” with the azide-terminated silica nanoparticles of a different size. This layer-by-layer growth is demonstrated to produce stable covalently-bound multilayers of nearly perfect structure over macroscopic solid substrates. The formation of stable covalent bonds is confirmed spectroscopically and the stability of the multilayers produced is tested by sonication in a variety of common solvents. The 1-, 2- and 3-layer structures are interrogated by electron microscopy and atomic force microscopy and the thickness of the multilayers formed is fully consistent with that expected for highly efficient monolayer formation with each cycle of growth. This approach can be extended to include a variety of materials deposited in a predesigned sequence on different substrates with a highly conformal filling.

Keywords

nanoparticle surface functionalization; monolayer formation; “click chemistry”; SEM

1. INTRODUCTION

Layered structures have been a target of intense research for many decades. For example, the ability to produce exceptional conformal filling over the high aspect ratio features

*Corresponding author, Department of Chemistry and Biochemistry, University of Delaware, Newark, DE 19716, USA; andrewt@udel.edu, Ph.: (302) 831-1969, Fax: (302) 831-6335.

#Y. L, M. G. W., and T. J. M. contributed equally to this work

needed in microelectronics has been based on the formation of targeted strong chemical bonds in the course of atomic layer deposition (ALD) (see reviews [1, 2] and multiple references therein) and the need for high-level control at the slightly larger scale for applications such as photoresist formation or metalorganic layer growth has been realized in molecular layer deposition (MLD) [3–6] processes. Both approaches utilize surface-limited reactions to form a layer of one atom to several atomic lengths thick that are perfectly suitable for a wide variety of applications. The main advantage of both methods is in atomic- and molecular level precision for the multilayers created. One of the main disadvantages is that the growth rate and the size of the building elements are very limited.

At the same time, layered materials with structural fragments of nanometers to tens of nanometers in size are needed for applications such as spintronics, specifically tunnel magnetoresistance [7], heterogeneous catalysis [8], magnetic materials [9], solar energy conversion with photoelectrochemical cells [10, 11] and many more. The formation of such films and materials using lithography or ALD and MLD methods is a very complex and expensive task.

Here we report the formation of multilayer systems based on *nearly complete monolayers* of nanoparticles covalently bound to a solid support in a self-limited surface process that utilizes “click chemistry” based on a reaction between azide and alkyne functionalities to form a triazole ring according to a general scheme shown in Figure 1. It is appropriate to term this approach as nanoparticle layer deposition (NPLD), in analogy to ALD and MLD.

Conceptually, similar approaches have been envisioned for a number of systems [12, 13], including covalent [14] or guest-host interactions [15]; however, achievement of a nanoparticle multilayer system in which each single layer is comprised of a *complete* monolayer has so far remained elusive.

On the other hand, high coverage can sometimes indeed be achieved by more traditional and well established approaches to layer-by-layer growth [16]. It should be emphasized that the process described here is fundamentally different from what is commonly referred to as layer-by-layer (LBL), where polymer layers [17, 18], polyelectrolytes [19], nanoparticle-incorporated materials [20–22], and supramolecular thin films [23] are deposited based on a continuous polymer film formed by a variety of deposition methods. Although useful in various applications, these approaches often involve polymers or fibers as alternate layers, which not only determine the properties of a resulting composite multilayer but also suggest that conformal filling with such processes is very difficult.

The proposed NPLD strategy takes advantage of the traditional LBL techniques but employs the approach that is rooted more in ALD and MLD. An excellent review of the recent achievements in all of these methods [16] compares recent developments in LBL techniques to advances in ALD or MLD.

The general approach described here can be utilized to form continuous layers consisting of nanoparticles of nanometers to microns in size, made of a variety of materials, and constructed in a variety of shapes. Most importantly, compared to other currently used

techniques for construction of relatively thick layers, the proposed process should lead to a conformal filling of intricate features, as well as flat surfaces.

In order to demonstrate the feasibility of such an approach, the complete monolayer-by-complete monolayer formation was performed using silica particles of different sizes with very narrow size distribution, so that the completion and quality of the layers could be monitored straightforwardly with microscopic analytical techniques. The chemistry was followed where appropriate with infrared spectroscopy and X-ray photoelectron spectroscopy (XPS) to confirm *covalent* bonding.

The *interlayer* bonding described here is based on the application of a copper-catalyzed "click reaction" between azide and alkyne functional groups to form the triazole ring in a cycloaddition process. Although a number of coupling processes are available for similar strategies, this high-yield "click reaction" is extremely selective [24, 25]. Furthermore, the triazole ring formed is highly stable against subsequent interactions [24]. Thus, this reaction has been applied in a variety of different fields, for example in drug delivery [24, 26, 27], polymer, and material science [28–31], making it universally acceptable for a wide range of applications. In fact, in an approach similar to MLD, Such *et al.* has employed this "click reaction" to create a layered film of covalently-bound polymers [25].

From a perspective of designing 3-dimensional materials with predesigned properties in a controlled fashion, continued efforts have been reported for the synthesis and characterization of cluster-assembled materials which can be tailored to exhibit collective properties unlike those of their individual components [32, 33]. Functionalized nanoparticles can be assembled together to form composite materials including the assemblies of inorganic nonmagnetic nanoparticles [13, 31, 34, 35] and magnetic nanoparticles that were recently explored [36–39]. For monolayer formation, Toulemon *et al*. reported that magnetic iron oxide nanoparticles could be assembled on solid substrates through "click chemistry" to form a *single* layer [39] and Kinge *et al.* has demonstrated the use of this "click reaction" to attach a layer of magnetic nanoparticles to a surface in pre-determined patterns through microcontact printing [37]. Upadhyay *et al.* has used this reaction to build layers of functionalized metallic nanoparticles starting with an alkyne-terminated solid substrate and demonstrated the possibility of multilayer formation and general applicability of this approach to a set of substrates and nanoparticles [13]. This last publication targeted the use of multilayer systems for electrocatalytic applications and proposed a well-conceived roadmap for building such multilayers. The synthesized structures performed well in the processes; however, only limited coverages were achieved most of the time both for monolayers and for multilayers, with parts of the surface covered with nearly close-packed monolayers and at the same time some empty or low-coverage areas. In addition, controlling the completion of a monolayer without depositing additional layers seems to be difficult. To overcome these issues, a modified surface preparation procedure based on a sonication-assisted reaction rather than self-assembly followed by chemical modification, is offered in this work. Carefully selected chemical pathways for modification of the nanoparticle surfaces, the use of nanoparticles of different sizes to confirm the formation of complete monolayers within the multilayer system and to rule out simultaneous deposition of multiple

layers in a single step, and spectroscopic confirmation of the covalent bonding of the nanoparticles are presented.

It should be pointed out that the properties of multilayered materials and individual layers can be altered by ALD-like reactions between pre-assembled nanoparticles and small chemical compounds during the deposition process [40]. This observation and previous experience in surface modification of solid substrates with buckyballs [41], biomolecules [42, 43], and nanoparticles [42] can be expanded for surface functionalization of silica nanoparticles and their deposition on a gold-coated substrate in a layer-by-layer manner. Again, it should be emphasized that this is not a process of self-assembly but rather a chemically-driven self-limiting process. Thus, the formation of the first stable layer with high coverage is the first task. Then, this very high-coverage layer is used as a platform for nanoparticle layer deposition of silica nanoparticles of different sizes in a second *complete* monolayer to form a continuous stable layered film. Thus, the proposed NPLD process relies on a chemical property of a single nanoparticle as a building block for producing multilayered structures based on completion of each monolayer within them.

2. EXPERIMENTAL DETAILS

2.1. Sample Preparation

Prefabricated gold substrates (1000 Å gold thickness on silicon wafer support with titanium adhesion layer, Sigma Aldrich) were cleaned by immersing the substrate into piranha solution (1:3 (by volume) hydrogen peroxide (30%, Fisher Scientific):concentrated sulfuric acid (98%, Fisher Scientific)) for 5 min followed by immersion in ultrapure water (18 MΩ·cm, Quantum EX, EMD Millipore) for 5 min. The substrate was then washed with HCl (37%, Fisher Scientific), water, ethanol (200 proof, Decon Laboratories, Inc.) and then dried under a flow of nitrogen gas. The clean Au substrate was immersed in a 1 mM solution of 11-azido-undecanethiol (96%, Krackeler Scientific, Inc. or synthesized following a previously established procedure) [44] in ethanol for 24–36 hours in the dark to produce the azide-terminated monolayer on Au substrate. The surface was then washed with ethanol, methylene chloride (99.9%, Fisher Scientific), and water, and dried under a flow of nitrogen gas. A titration experiment to react surface azide was performed by immersing the gold substrate into 4:1 methanol:water (by volume) with ~15 mM 5-hexynoic acid (97%, Sigma-Aldrich) in methanol (99.9%, Fisher Scientific). Catalytic amounts of copper sulfate pentahydrate (>99%, Fisher Scientific) and sodium ascorbate (>99%, Fisher Scientific) were added to the solution and the mixture was sonicated for 24 hours, followed by washing with ethanol, methylene chloride, water, and ethanol.

2.2. Alkyne-Terminated Nanoparticle Preparation

Surface functionalization of 80 nm silica nanoparticles (dried, NanoComposix) to prepare alkyne functional groups was based on a previously published procedure [45]. 218 μL of tetramethyl orthosilicate (98%, Sigma-Aldrich) and 218 μL of 4-pentyn-1-ol (97%, Sigma-Aldrich) were dissolved in 10 mL of toluene (<99%, Fisher Scientific). The resulting solution was stirred at room temperature for 24 hours. The 80 nm silica nanoparticles were dispersed into 2 mL of toluene and added to the solution. The mixture was stirred at 80ºC for

24 hours to form the alkyne-terminated silica nanoparticles. The resulting nanoparticles were washed in methanol five times followed by dispersion into methanol for further use.

2.3. Azide-Terminated Nanoparticle Preparation

The 50 nm silica nanoparticles (10 mg/mL, dispersed in water, NanoComposix) exchanged solvents by dispersion in a series of ethanol/water mixtures (1:1, 3:2, 1:0 and 1:0) [46], so that the solvent could be changed from water to ethanol. The solvent was then exchanged to toluene by a series of toluene/ethanol solvents (1:1, 3:2, 1:0 and 1:0) to produce 50 nm silica nanoparticles dispersed in toluene. The azide-termination was performed similarly to that for alkyne-terminated silica nanoparticles. 218 μL of tetramethyl orthosilicate and 36 μL of 2-azidoethanol (95%, MolPort) were dissolved into 10 mL of toluene. The resulting solution was stirred at 80ºC for 24 hours and used without further purification. The 50 nm silica nanoparticles were dispersed into 2 mL of toluene and added to the solution. The mixture was then stirred and refluxed for 24 hours to form the azide-terminated silica nanoparticles. The resulting nanoparticles were then washed in methanol five times followed by dispersion into methanol for further use.

2.4. First Nanoparticle Layer Deposition via “Click Chemistry”

The gold substrate was immersed into 4:1 methanol:water (by volume) with ~3 mg/mL 80 nm alkyne-terminated silica nanoparticles. Catalytic amounts of copper sulfate pentahydrate and sodium ascorbate were added to the system. The mixture was then sonicated for 24 hours, followed by washing with ethanol, methylene chloride, water, and ethanol, and further sonicated for 30 min in ethanol to remove physically adsorbed nanoparticles and remaining catalyst. A titration experiment to react remaining azide was performed by immersing the first-layer sample into 4:1 methanol:water (by volume) with ~15 mM 5-hexynoic acid in methanol. Catalytic amounts of copper sulfate pentahydrate and sodium ascorbate were added to the solution and the mixture was sonicated for 24 hours, followed by washing with ethanol, methylene chloride, water, and ethanol to remove physically adsorbed particles and remaining copper-containing species.

2.5. Second Nanoparticle Layer Deposition via “Click Chemistry”

The gold substrate modified with the first layer of 80 nm silica nanoparticles with alkyne functional group was incubated with a drop of azide-terminated 50 nm silica nanoparticles in 4:1 methanol:water (by volume) solvent until dry. The sample was then rinsed with ethanol, methylene chloride, water, ethanol and further sonicated for 30 min in ethanol to remove the physically adsorbed nanoparticles.

2.6. Third Nanoparticle Layer Deposition via “Click Chemistry”

The prepared double layer of nanoparticles on the gold wafer was covered with a drop of alkyne-terminated 80 nm silica nanoparticles in 4:1 methanol:water (by volume) with trace amount of copper sulfate pentahydrate and sodium ascorbate catalysts until dry. The sample was then rinsed with ethanol, methylene chloride, water, and ethanol and sonicated for 30 min in ethanol to remove the physically adsorbed nanoparticles.

2.7. Characterization Methods

Single point attenuated total reflectance Fourier transform infrared (ATR FT-IR) spectroscopy measurements were performed on a Bruker Optics (Billerica, MA) Vertex 70 FT-IR with a Bruker Hyperion 2000 Microscope attachment and liquid nitrogen cooled MCT detector. The Hyperion microscope is equipped with a dedicated single-point ATR attachment for surface analysis. Each spectrum was produced from 256 scans at a resolution of 4 cm^{-1}, and at a spectral range from 4000 cm^{-1} to 600 cm^{-1}. The functionalized surfaces and nanoparticle deposited surfaces were referenced against a gold surface sonically cleaned in ethanol.

Two scanning electron microscopes (SEM), JEOL JSM-7400F and Zeiss Auriga 60, were utilized to investigate the morphology of the nanoparticles on the surface as well as a cross-sectional view of the deposited nanoparticles. The control experimental images were taken in the JEOL JSM-7400F, and the images were collected with accelerating energy of 15 keV and a working distance of 8.0 mm. All experimental images were collected by secondary electrons (in-lens detector) with an accelerating energy of 3 keV and a working distance of 5.0 mm. In order to investigate the nanoparticle layer thickness, a gallium focused ion beam (FIB) was used to etch away nanoparticles. The gallium beam had an energy of 30 kV and a current of 120 pA. The polished samples were then placed at a 65° angle (which is the limit of the SEM/FIB stage), and images were recorded.

Tapping mode atomic force microscopy (AFM) was performed on a Veeco Multimode SPM with a Nanoscope Dimension 3100 controller. BS-Tap 300Al tips (Budget Sensors) with a force constant of 40 N/m and a drive frequency of 300 kHz were used to measure the topography of the samples. The images were 512 by 512 pixels and were analyzed using Gwyddion software [47].

The X-ray photoelectron spectroscopy studies were performed on a PHI 5600 X-ray Photoelectron Spectrometer equipped with an Al Kα X-ray source (hν=1486.6 eV) at a 45° take- off angle. The measurements were performed in a vacuum chamber with a base pressure of 1.3×10^{7} Pa. Before loading for XPS measurements, ethanol was used to clean the surface. No additional cleaning procedures were used within the vacuum chamber. Survey spectra were collected from 0 to 1000 eV binding energy. High-resolution spectra were collected with a pass energy of 20 eV, an energy step size of 0.1 eV, and 15 passes per cycle. The Au $4f_{7/2}$ peak at 83.8 eV was used to calibrate the spectra. CasaXPS software (Version 2.3.5) was used for data processing and peak fitting.

The Gaussian 09 Suite [48] of programs was used to perform density functional theory (DFT) calculations using B3LYP functional and a 6–311 +G-(d,p) basis set. Geometry optimization and prediction of the core level XPS spectra for the N 1s region were performed. The azide-terminated self-assembled monolayer (SAM) was modeled using optimized 11-azido-undecanethiol, the first layer reaction was modeled using the optimized triazole-linked 4-pentyn-1-ol and 11-azido-undecanethiol, and the two layer sample was modeled using the optimized triazole-linked 4-pentyn-1-ol and 2-azidoethanol. The computationally predicted XPS spectra were calibrated with a correction factor of 8.76 eV for the 6-311+G-(d,p) basis set, based on our previous work [49].

3. RESULTS AND DISCUSSION

3.1. Formation of the First Layer of Nanoparticles

In order to image the surface and determine surface coverage, scanning electron microscopy was performed to follow the physical adsorption process and chemical attachment of silica nanoparticles to the gold substrate. The experiments with nanoparticles without complimentary chemical functionalities lead to physisorption, where the physisorbed particles could be easily removed by solvents or by sonication. To exclude the nonspecific binding, a number of control experiments were performed for alkyne-terminated silica nanoparticles sonicated in methanol solvent with Au substrate with and without washing processes. Only the formation of strong chemical bonds through the triazole ring keeps the layered system stable. In order to confirm this behavior, two control experiments were performed: (1) to show the importance of the complimentary chemistry, and (2) to show the stable nature of the triazole ring. These experiments, along with topography verification for a single layer generated by a “click chemistry” reaction by atomic force microscopy, are summarized in Figure 2.

For physical adsorption of silica nanoparticles, a small number of nanoparticles were observed on the surface, as shown in Figure 2(a); however, after washing and sonication, a pristine surface without any nanoparticles deposited is observed, as demonstrated in Figure 2(b). When compared to the “click chemistry” procedure in Figure 2(c), it is evident that there is a chemical attachment through the “click reaction” leading to the formation of a strongly bound monolayer. The nanoparticle monolayer and multilayers formed as demonstrated below are very stable with respect to washing with standard solvents and sonication. Two points are very important here: 1) the plan view shown in Figure 2(c) corresponds to a monolayer; and 2) the formation of strong chemical bonds as a result of “click reaction” should be confirmed independently via spectroscopy studies. The AFM image in Figure 2(d) is recorded on a fringe of the monolayer, where a substantial amount of empty space (free of nanoparticles) is observed. The image and inset confirm that only a single monolayer is observed and that the distance between the centers of the nanoparticles corresponds to a full size with no noticeable changes. Based on these images the coverage of the first monolayer was determined, as described in detail below.

The SEM investigation of the monolayer and multilayer formation will be addressed next, and the spectroscopic confirmation of chemical reaction will follow.

3.2. Deposition of Sequential Layers of Complementarily-Functionalized Nanoparticles

Following the deposition of the first layer of 80 nm functionalized nanoparticles, the second layer was chosen to be 50 nm azide-functionalized nanoparticles. A difference in size allows for a simple verification of the deposition process and the completeness of the formation of the second layer by SEM. Additional studies with a focused ion beam to etch out and polish the samples were used to determine the thickness of the samples over a large area of uniform nanoparticle coverage. The summary of the obtained results is given in Figure 3. In Figure 3(a), the plan view of the first layer of 80 nm alkyne-terminated nanoparticle is shown. From the number of nanoparticles observed by SEM, the coverage of the first layer is calculated to

be 84±8%, based on the assumption that 100% coverage refers to a full single layer of particles in a hexagonal close-packed formation. This is excellent even compared to a single cycle of ALD [50]. It has to be emphasized again that the silica nanoparticles were not deposited through the self-assembly process; they were randomly reacting with the surface to form covalent linkages, and the first layer was formed in a sonication-assisted process. To confirm that self-assembly does not play a deciding role in the formation of a monolayer, Figure 4 shows randomly-distributed covalently bound nanoparticles on the same substrate at low coverage. Thus, the ultimate coverage achieved is extremely high and the reaction is very efficient. Figure 3(b) shows the cross sectional view of the nanoparticle deposition. Here, one can see (from bottom to top) the silicon substrate, a thin gold layer, and the single layer of SiO_2 nanoparticles. The height of 80 nm is what is expected for a single layer, consistent with the AFM image in Figure 2(d).

Following the deposition of the first layer of 80 nm alkyne functionalized nanoparticles, the 2-layer system with the second layer of azide-functionalized 50 nm nanoparticles is shown in Figures 3(c–d). Such a difference in size allows for a simple verification of the deposition process and the completeness of the formation of the second layer by SEM. As shown in Figure 3(c), the nearly complete second layer of 50 nm silica nanoparticles is formed on a top of the first layer, with a calculated coverage of 94% based on the absolute area of the substrate (compared to the ideal computed close-packed layer), and the bilayer system is just as stable as the first monolayer. The high coverage of the second layer is reproducible but the exact per cent coverage in this case does not reflect the fact that this second layer is deposited on top of the first and not onto a flat surface. In Figure 3(d), the thickness of the bilayer shown in Figure 3(c) is 130 nm, which is fully consistent with depositing the second layer of 50 nm nanoparticles on top of a layer of 80 nm nanoparticles. Since the sizes of the nanoparticles within the first layer are larger than those of the second layer, and since the attachment is driven by a chemical reaction rather than self-assembly, the deposition process does not lead to any specific packing of the second layer.

The same approach was tested to produce the third layer with 80 nm alkyne-terminated nanoparticles and leads to a high-coverage layer (approximately 94% coverage, similarly to the coverage of the second layer) formation shown in Figure 3(e–f). Figure 3(e) shows a surface (plan) view with high coverage and Figure 3(f) demonstrates that the thickness of the 3-layer system reaches 210 nm, which is exactly what would be expected for a layer of 50 nm nanoparticles sandwiched between two layers of 80 nm nanoparticles. In all of these studies, the nanoparticle monolayer and multilayers formed through “click chemistry” are very stable. Washing with any combination of the standard solvents or sonication in methanol did not remove any particles and did not affect the coverage of this first layer. The size of the nanoparticles used, however, does appear to influence the coverage. In general, smaller diameter nanoparticles seem to result in higher surface coverage when applied on top of a first layer of larger diameter particles. This became evident when 200 nm nanoparticles were tested in place of the 50 nm particles to form a second layer, producing lower surface coverage and even suggesting damage to the first layer by the sonication-assisted process.

3.3. Spectroscopic Confirmation of "Click Chemistry" for NPLD

Single point attenuated total reflectance Fourier transform infrared spectroscopy was used to prove chemical attachment of nanoparticles to the azide-terminated gold surface. Figure 5 shows the informative infrared regions of these data. All spectra are referenced to an ethanol-cleaned gold substrate. Figure 5(a) shows the azide-terminated gold surface. An intense peak observed at 2096 cm^{-1} is fully consistent with the stretching of the azide functional group for the 11-azido-undecanethiol on gold substrate [44]. At the same time, symmetric and asymmetric CH_2 stretching peaks are observed at 2854 cm^{-1} and 2925 cm^{-1}, respectively. These peaks are indicative of a partially-ordered self-assembled alkyl overlayer [51–53]. Some degree of disorder in the alkyl overlayer is expected because the ATR FT-IR tip, which is orders of magnitude larger than the layer, comes into physical contact with the surface, disrupting the overlayer. Figure 5(c) shows the infrared spectrum collected following the deposition of the first layer of nanoparticles. Here, the intensity of the azide peak is decreased substantially, since the terminating layer is now consisted of the alkyne-terminated nanoparticles. At the same time, it is obvious that not all the azide groups would react following the deposition of the first layer of nanoparticles. It has been recently proposed [54] that the mechanism for the copper-catalyzed reaction involves the interaction of two copper centers directly with the alkyne functionality, instead of one, as had been suggested previously [55]. If this is the case, it is likely that the formation of the triazole ring is hindered by the bulk of the copper-alkyne intermediate which would need to insert into the ordered monolayer. This steric limitation would undoubtedly result in the presence of unreacted azide. The symmetric and asymmetric CH_2 stretches are still present at 2854 cm^{-1} and 2927 cm^{-1}, which are indicative of a slightly disordered system [51–53, 56] that now combines the SAM on gold substrate and the alkyl groups of the functionalized nanoparticles. This is expected since the alkyne-termination of functionalized nanoparticles is no longer completely ordered. That is, the geometry of the nanoparticle (compared to a flat substrate) makes its functionalization with a SAM result in a slightly disordered molecular layer. Additionally, the disorder of the alkyl chains in the molecular functionalized layers likely originates from a relatively short alkyl chain, although the alkyne termination could further be used to react with azide-terminated silica nanoparticles.

In order to prove that the observed 2096 cm^{-1} peak corresponds to azide group, the titration experiments with 5-hexynoic acid were performed on the azide-terminated SAM on gold and on the sample covered with one monolayer of nanoparticles. In both cases the peak at 2096 cm^{-1} disappeared completely, as shown in Figure 5(b) and (d), respectively. This peak appears again for a system built by depositing two layers of complementarily functionalized nanoparticles shown in Figure 5(e).

The presence of the ≡C-H vibration indicative of the alkyne-functionalized particles attachment is proven by the presence of a weak peak at 3267 cm^{-1} following 1st and 3rd layer deposition, consistent with the expected alkyne C-H vibrations [57] within an organic monolayer. Thus, despite the complexity of the system under investigation, infrared spectroscopy confirms the chemical reaction following deposition of each layer of nanoparticles and the availability of the azide functional groups on the SAM-functionalized gold surface, as well as on the even layers of nanoparticles.

The X-ray photoelectron spectroscopy studies summarized in Figure 6 also show evidence of the chemical attachment of the nanoparticles through “click chemistry”. All of the peaks were calibrated to the Au $4f_{7/2}$ peak at 83.8 eV as opposed to calibration against the C 1*s* peak at 284.6 eV because the alkyne functionality is present in some samples and could influence the C 1*s* peak position. Figures 6(a,e) show the azide-terminated gold surface for the C 1*s* and N 1*s* regions, respectively. In the C 1*s* region, there is a large peak at 284.6 eV with two small peaks at 286.0 V and 288.5 eV. These peaks can be assigned to C-C bonds [58, 59], C-N/C-O bonds [60], and C=O bonds [60, 61], respectively. The oxidized species are present since the samples were transported through the air and adventitious carbon adsorbed onto the sample. In the N 1*s* region, there are two features that can be deconvoluted to three peaks present in the spectra. These three peaks correspond to the three different types of nitrogen present in the sample. The three peaks located at 403.4 eV, 400.6 eV, and 400.0 eV correspond to the –N=***N***=N, –N=N=***N***, and –***N***=N=N (bolded and italicized nitrogen), respectively. The spectrum also lines up very well with the previous work on “click chemistry” with iron nanoparticles [36]. These two regions show that there is azide present on the surface that is a perfect starting point with minimal oxidation.

Figures 6(b,f) show the C 1*s* and N 1*s* spectral regions following the first layer deposition of the 80-nm alkyne-terminated nanoparticles onto the azide-terminated surface, respectively. Again there are peaks at 284.6 eV, 286.0 eV, and 288.5 eV within the C 1s spectral range, which can be assigned the same way as for the starting surface. There is also an additional peak at 284.0 eV, which likely corresponds to the C≡C of the alkyne and could also be indicative of the C=C bond in the triazole ring. A broad feature observed in the N 1*s* region in Figure 6f can be deconvoluted into three peaks at 401.5 eV, 400.4 eV, and 399.4 eV, and are assigned to the –C-***N***-N-, -N-***N***=N-, and –N=***N***-C- (again, bolded and italicized) nitrogen atoms, respectively. This assignment is based on the previous studies [36, 62, 63] of the “click reaction” in similar systems and also on the computational prediction shown in color immediately underneath this plot. There is a possibility that azide functionality may still be present (with incomplete nanoparticle coverage), as shown above in the FT-IR studies. Again, this is very similar to the iron nanoparticle “click chemistry” study where a nearly identical broad feature following the “click reaction” was reported [36]. These spectra confirm that there is high coverage of nanoparticles deposited by the “click reaction” onto a functionalized substrate and that this first layer provides an acceptable starting point for the next nanoparticle layer deposition.

Figures 6(c,g) show the C 1*s* and N 1*s* regions following deposition of the 50 nm azide-terminated nanoparticles onto the first 80 nm alkyne-terminated nanoparticle layer, respectively. The chemical identity of all the functionalities within this complex system is nearly impossible; however, the peaks at 284.0 eV, 284.6 eV, 286.0 eV, and 288.5 eV in the C 1*s* spectral region correspond to the same respective carbon-containing functional groups as described above for the starting substrate and the same surface following chemical deposition of the first layer of nanoparticles. The higher overall intensity of the N 1*s* spectral region is consistent with the presence of the second layer of the nanoparticles terminated with azide functionality. A possible fit combining the 6 peaks that are perfectly aligned with the results in Figure 6(e–f) and an extra peak at 407.1 eV which likely corresponds to the

oxidized nitrogen species [64] since the sample is transported to the XPS chamber in ambient environment is provided immediately underneath the plot. This complex picture is expected, since this layer should be a combination of all the layers and functionalities; that is, this layer should have the terminated azide functionality (peaks at 403.4 eV, 400.6 eV, and 400.0 eV) while containing the triazole ring obtained through the “click chemistry” (peaks at 401.5 eV, 400.4 eV, and 399.4 eV). Finally, following the deposition of the third layer of nanoparticles, the complexity of the features observed by XPS increases even further as the system becomes more disordered as more layers are added and as nitrogen species may become trapped between the particles; however, the intensities of the features observed are consistent with the expected nearly-complete layer by layer chemical deposition. It should be added that, when performed properly, the washing procedure was shown to efficiently remove copper contamination from the surface following the “click reaction”, as confirmed by XPS.

Thus, the XPS spectra confirm that the “click chemistry” results in chemically bound layers of nanoparticles and can be used to deposit the nanoparticles layer by layer. The complexity of the system prevents from exact identification of all the chemical species present in the multilayer system by XPS because of multiple species involved, screening by the nanoparticles deposited, and likelihood of oxidation of some of the nitrogen-containing species during the sample transfer in ambient.

4. CONCLUSIONS AND PERSPECTIVES

This work showcases a modified deposition scheme for efficiently building multilayer systems of nanoparticles on solid substrates based on sonication-assisted chemical reaction leading to the formation of covalent linkages rather than based on a process of self-assembly. It was proposed and tested as a nanoparticle layer deposition approach based on a “click reaction” stimulated by sonication. A nearly complete high-coverage first layer was formed by this approach using an azide-functionalized gold substrate and alkyne-terminated silica nanoparticles. This deposition step leaves a sufficient number of alkyne groups to react further with azide-terminated silica nanoparticles to form a high-coverage second layer. The feasibility of continuing this process was tested for the third layer as well. This process of growth is fundamentally different from current layer-by-layer growth methods involving nanoparticles and is much more similar to the molecular and atomic growth by MLD and ALD, respectively, making this approach a feasible method for growth of controlled layered systems with minimal organic contamination and with potentially high conformal filling. As the process is not driven by self-assembly but rather by surface chemical reactions, this general approach opens up a number of opportunities for three-dimensional design of architectures based on chemically driven attachment.

Further mechanistic studies are under way for uncovering the reasoning behind the high-coverage, high-precision monolayer formation based on the starting azide-terminated surface as opposed to the alkyne-terminated substrates. The idea was tested previously but not pursued for efficient multilayer formation based on complete monolayers [13]. However, this starting point might be very important, since the interaction of copper catalyst with the alkyne group is required for successful implementation of the “click chemistry” used here. It

was recently proposed that this interaction requires the involvement of not one but two copper (I) centers [54], making the resulting intermediate very bulky to form on an alkyne-terminated flat surface. However, this intermediate could form much more easily on a less-ordered surface of functionalized nanoparticles, thus leading to a more efficient reaction for azide-terminated flat starting substrates with alkyne-terminated nanoparticles compared to that for alkyne-terminated starting surface and azide-terminated nanoparticles.

Acknowledgments

This work is supported by National Science Foundation (CHE 1057374). Acknowledgment is also made to the donors of the Petroleum Research Fund, administered by the American Chemical Society, for partial support of this research. We acknowledge the support of the NIGMS 1 P30 GM110758 grant for the support of core instrumentation infrastructure at the University of Delaware. The authors would like to thank K. Booksh, L. Kegel, and D. Boyne (Department of Chemistry, University of Delaware) with their support of single point ATR instrument. The authors would also like to thank R. Opila and K. Jones for XPS support as well as J. Koh and E. Zhang (Department of Chemistry, University of Delaware) for their help with synthesis of 11-azido-undecanethiol.

References

1. Parsons GN, Elam JW, George SM, Haukka S, Jeon H, Kessels WMM, Leskelä M, Poodt P, Ritala M, Rossnagel SM. History of atomic layer deposition and its relationship with the American Vacuum Society. J Vac Sci Technol A. 2013; 31(5):050818.
2. Bakke JR, Pickrahn KL, Brennan TP, Bent SF. Nanoengineering and interfacial engineering of photovoltaics by atomic layer deposition. Nanoscale. 2011; 3(9):3482. [PubMed: 21799978]
3. George SM, Yoon B, Dameron AA. Surface Chemistry for Molecular Layer Deposition of Organic and Hybrid Organic-Inorganic Polymers. Acc Chem Res. 2009; 42(4):498. [PubMed: 19249861]
4. Adamczyk NM, Dameron AA, George SM. Molecular Layer Deposition of Poly(*p*-phenylene terephthalamide) Films Using Terephthaloyl Chloride and *p*-Phenylenediamine. Langmuir. 2008; 24:2081. [PubMed: 18215079]
5. Zhou H, Bent SF. Molecular Layer Deposition of Functional Thin Films for Advanced Lithographic Patterning. ACS Appl Mater Interfaces. 2011; 3(2):505. [PubMed: 21302918]
6. Bent S, Loscutoff PW, Clendenning S. Fabrication of Organic Thin Films for Copper Diffusion Barrier Layers Using Molecular Layer Deposition. Proceedings of Materials Research Society. 2010:1249-F02–03.
7. Yuasa S, Djayaprawira DD. Giant tunnel magnetoresistance in magnetic tunnel junctions with a crystalline MgO(0 0 1) barrier. J Phys D: Appl Phys. 2007; 40(21):R337.
8. Cuenya BR. Synthesis and catalytic properties of metal nanoparticles: Size, shape, support, composition, and oxidation state effects. Thin Solid Films. 2010; 518(12):3127.
9. Guo J, Yang W, Wang C. Magnetic Colloidal Supraparticles: Design, Fabrication and Biomedical Applications. Adv Mater (Weinheim, Ger). 2013; 25(37):5196.
10. Li Z, Luo W, Zhang M, Feng J, Zou Z. Photoelectrochemical cells for solar hydrogen production: current state of promising photoelectrodes, methods to improve their properties, and outlook. Energ Environ Sci. 2013; 6(2):347.
11. Ovits O, Tel-Vered R, Baravik I, Wilner OI, Willner I. Photoelectrochemical cells based on bis-aniline-crosslinked CdS nanoparticle-carbon nanotube matrices associated with electrodes. J Mater Chem. 2009; 19(41):7650.
12. Chao-Hua X, Shun-Tian J, Jing Z, Jian-Zhong M. Large-area fabrication of superhydrophobic surfaces for practical applications: an overview. Sci Technol Adv Mater. 2010; 11(3):033002.
13. Upadhyay AP, Behara DK, Sharma GP, Bajpai A, Sharac N, Ragan R, Pala RGS, Sivakumar S. Generic Process for Highly Stable Metallic Nanoparticle-Semiconductor Heterostructures via Click Chemistry for Electro/Photocatalytic Applications. ACS Appl Mater Interfaces. 2013; 5(19): 9554. [PubMed: 24018108]

14. Amigoni S, Taffin de Givenchy E, Dufay M, Guittard F. Covalent Layer-by-Layer Assembled Superhydrophobic Organic-Inorganic Hybrid Films. Langmuir. 2009; 25(18):11073. [PubMed: 19601564]
15. Crespo-Biel O, Dordi B, Reinhoudt DN, Huskens J. Supramolecular Layer-by-Layer Assembly: Alternating Adsorptions of Guest- and Host-Functionalized Molecules and Particles Using Multivalent Supramolecular Interactions. J Am Chem Soc. 2005; 127(20):7594. [PubMed: 15898811]
16. Borges J, Mano JF. Molecular Interactions Driving the Layer-by-Layer Assembly of Multilayers. Chem Rev. 2014; 114(18):8883. [PubMed: 25138984]
17. Chen W, McCarthy TJ. Layer-by-Layer Deposition: A Tool for Polymer Surface Modification. Macromolecules. 1997; 30(1):78.
18. Khademhosseini A, Suh KY, Yang JM, Eng G, Yeh J, Levenberg S, Langer R. Layer-by-layer deposition of hyaluronic acid and poly-l-lysine for patterned cell co-cultures. Biomaterials. 2004; 25(17):3583. [PubMed: 15020132]
19. Zhang J, Senger B, Vautier D, Picart C, Schaaf P, Voegel JC, Lavalle P. Natural polyelectrolyte films based on layer-by layer deposition of collagen and hyaluronic acid. Biomaterials. 2005; 26(16):3353. [PubMed: 15603831]
20. Dubas ST, Kumlangdudsana P, Potiyaraj P. Layer-by-layer deposition of antimicrobial silver nanoparticles on textile fibers. Colloids Surf, A. 2006; 289(1–3):105.
21. Jiang C, Tsukruk VV. Freestanding Nanostructures via Layer-by-Layer Assembly. Adv Mater (Weinheim, Ger). 2006; 18(7):829.
22. Gao Y, Qi J, Zhang J, Kang S, Qiao W, Li M, Sun H, Zhang J, Ariga K. Fabrication of both the photoactive layer and the electrode by electrochemical assembly: towards a fully solution-processable device. Chem Commun. 2014; 50(72):10448.
23. Nishiyama F, Yokoyama T, Kamikado T, Yokoyama S, Mashiko S. Layer-by-layer growth of porphyrin supramolecular thin films. Appl Phys Lett. 2006; 88(25):253113.
24. Kolb HC, Sharpless KB. The Growing Impact of Click Chemistry on Drug Discovery. Drug Discovery Today. 2003; 8(24):1128. [PubMed: 14678739]
25. Such GK, Quinn JF, Quinn A, Tjipto E, Caruso F. Assembly of Ultrathin Polymer Multilayer Films by Click Chemistry. J Am Chem Soc. 2006; 128(29):9318. [PubMed: 16848452]
26. Lipinski C, Hopkins A. Navigating Chemical Space for Biology and Medicine. Nature. 2004; 432(7019):855. [PubMed: 15602551]
27. Hjorringgaard CU, Vad BS, Matchkov VV, Nielsen SB, Vosegaard T, Nielsen NC, Otzen DE, Skrydstrup T. Cyclodextrin-Scaffolded Alamethicin with Remarkably Efficient Membrane Permeabilizing Properties and Membrane Current Conductance. J Phys Chem B. 2012; 116(26): 7652. [PubMed: 22676384]
28. Binder WH, Sachsenhofer R. 'Click' Chemistry in Polymer and Materials Science. Macromol Rapid Commun. 2007; 28(1):15.
29. Fournier D, Hoogenboom R, Schubert US. Clicking Polymers: a Straightforward Approach to Novel Macromolecular Architectures. Chem Soc Rev. 2007; 36(8):1369. [PubMed: 17619693]
30. Acikgoz S, Aktas G, Inci MN, Altin H, Sanyal A. FRET betvveen BODIPY Azide Dye Clusters within PEG-Based Hydrogel: A Handle to Measure Stimuli Responsiveness. J Phys Chem B. 2010; 114(34):10954. [PubMed: 20698507]
31. Peng J, Yu P, Zeng S, Liu X, Chen J, Xu W. Application of Click Chemistry in the Fabrication of Cactus-Like Hierarchical Particulates for Sticky Superhydrophobic Surfaces. J Phys Chem C. 2010; 114(13):5926.
32. Claridge SA, Castleman AW, Khanna SN, Murray CB, Sen A, Weiss PS. Cluster-Assembled Materials. ACS Nano. 2009; 3(2):244. [PubMed: 19236057]
33. Pelaz B, Jaber S, de Aberasturi DJ, Wulf V, Aida T, de la Fuente JsM, Feldmann J, Gaub HE, Josephson L, Kagan CR, Kotov NA, Liz-Marzán LM, Mattoussi H, Mulvaney P, Murray CB, Rogach AL, Weiss PS, Willner I, Parak WJ. The State of Nanoparticle-Based Nanoscience and Biotechnology: Progress, Promises, and Challenges. ACS Nano. 2012; 6(10):8468. [PubMed: 23016700]

34. Janczewski D, Tomczak N, Liu S, Han MY, Vancso GJ. Covalent Assembly of Functional Inorganic Nanoparticles by "Click" Chemistry in Water. Chem Commun. 2010; 46(19):3253.
35. Zhao J, Terfort A, Zharnikov M. Gold Nanoparticle Patterning on Monomolecular Chemical Templates Fabricated by Irradiation-Promoted Exchange Reaction. J Phys Chem C. 2011; 115(29):14058.
36. Liu Y, RamaRao N, Miller T, Hadjipanayis G, Teplyakov AV. Controlling physical properties of iron nanoparticles during assembly by "click chemistry". J Phys Chem C. 2013; 117(39):19974.
37. Kinge S, Gang T, Naber WJM, van der Wiel WG, Reinhoudt DN. Magnetic Nanoparticle Assembly on Surfaces Using Click Chemistry. Langmuir. 2011; 27(2):570. [PubMed: 21162518]
38. Zhao J, Spasova M, Li ZA, Zharnikov M. Ferromagnetic Cobalt Nanoparticles and Their Immobilization on Monomolecular Films and Chemical Templates. Adv Funct Mater. 2011; 21(24):4724.
39. Toulemon D, Pichon BP, Leuvrey C, Zafeiratos S, Papaefthimiou V, Cattoën X, Begin-Colin S. Fast Assembling of Magnetic Iron Oxide Nanoparticles by Microwave-Assisted Copper(I) Catalyzed Alkyne-Azide Cycloaddition (CuAAC). Chem Mater. 2013; 25(14):2849.
40. Dafinone MI, Feng G, Brugarolas T, Tettey KE, Lee D. Mechanical Reinforcement of Nanoparticle Thin Films Using Atomic Layer Deposition. ACS Nano. 2011; 5(6):5078. [PubMed: 21557541]
41. Zhang X, Teplyakov AV. Adsorption of C-60 Buckminster Fullerenes on an 11-Amino-1-Undecene-Covered Si(111) Substrate. Langmuir. 2008; 24(3):810. [PubMed: 18085804]
42. Liu Y, Chen JHE, Teplyakov AV. Chemical Passivation Processes for Biofunctionalization Schemes on Semiconductor Surfaces. Langmuir. 2012; 28(44):15521. [PubMed: 23025426]
43. Zhang X, Kumar S, Chen J, Teplyakov AV. Covalent Attachment of Shape-Restricted DNA Molecules on Amine-Functionalized Si(111) Surface. Surf Sci. 2009; 603(16):2445.
44. Collman JP, Devaraj NK, Chidsey CED. "Clicking" functionality onto electrode surfaces. Langmuir. 2004; 20(4):1051. [PubMed: 15803676]
45. Mader H, Li X, Saleh S, Link M, Kele P, Wolfbeis OS. Fluorescence Methods and Applications: Spectroscopy, Imaging, and Probes. Ann N Y Acad Sci. 2008; 1130:218. [PubMed: 18596351]
46. Rahman IA, Vejayakumaran P, Sipaut CS, Ismail J, Chee CK. Effect of the drying techniques on the morphology of silica nanoparticles synthesized via sol-gel process. Ceram Int. 2008; 34(8): 2059.
47. Nečas D, Klapetek P. Gwyddion: an open-source software for SPM data analysis. Central European Journal of Physics. 2012; 10(1):181.
48. Frisch, MJ.; Trucks, GW.; Schlegel, HB.; Scuseria, GE.; Robb, MA.; Cheeseman, JR.; Scalmani, G.; Barone, V.; Mennucci, B.; Petersson, GA.; Nakatsuji, H.; Caricato, M.; Li, X.; Hratchian, HP.; Izmaylov, AF.; Bloino, J.; Zheng, G.; Sonnenberg, JL.; Hada, M.; Ehara, M.; Toyota, K.; Fukuda, R.; Hasegawa, J.; Ishida, M.; Nakajima, T.; Honda, Y.; Kitao, O.; Nakai, H.; Vreven, T.; Montgomery, JA.; Peralta, JE.; Ogliaro, F.; Bearpark, M.; Heyd, JJ.; Brothers, E.; Kudin, KN.; Staroverov, VN.; Kobayashi, R.; Normand, J.; Raghavachari, K.; Rendell, A.; Burant, JC.; Iyengar, SS.; Tomasi, J.; Cossi, M.; Rega, N.; Millam, JM.; Klene, M.; Knox, JE.; Cross, JB.; Bakken, V.; Adamo, C.; Jaramillo, J.; Gomperts, R.; Stratmann, RE.; Yazyev, O.; Austin, AJ.; Cammi, R.; Pomelli, C.; Ochterski, JW.; Martin, RL.; Morokuma, K.; Zakrzewski, VG.; Voth, GA.; Salvador, P.; Dannenberg, JJ.; Dapprich, S.; Daniels, AD.; Farkas; Foresman, JB.; Ortiz, JV.; Cioslowski, J.; Fox, DJ. Gaussian 09, Revision B.01. Gaussian, Inc; Wallingford CT: 2009.
49. Leftwich TR, Teplyakov AV. Calibration of computationally predicted N 1s binding energies by comparison with X-ray photoelectron spectroscopy measurements. J Electron Spectrosc Relat Phenom. 2009; 175:31.
50. Wind RW, Fabreguette FH, Sechrist ZA, George SM. Nucleation period, surface roughness, and oscillations in mass gain per cycle during W atomic layer deposition on Al_2O_3. J Appl Phys. 2009; 105(7):074309.
51. Sieval AB, Linke R, Heij G, Meijer G, Zuilhof H, Sudholter EJR. Amino-terminated organic monolayers on hydrogen-terminated silicon surfaces. Langmuir. 2001; 17(24):7554.

52. Perring M, Dutta S, Arafat S, Mitchell M, Kenis PJA, Bowden NB. Simple methods for the direct assembly, functionalization, and patterning of acid-terminated monolayers on Si(111). Langmuir. 2005; 21(23):10537. [PubMed: 16262318]

53. Tian FY, Ni CY, Teplyakov AV. Integrity of functional self-assembled monolayers on hydrogen-terminated silicon-on-insulator wafers. Appl Surf Sci. 2010; 257(4):1314.

54. Worrell BT, Malik JA, Fokin VV. Direct Evidence of a Dinuclear Copper Intermediate in Cu(I)-Catalyzed Azide-Alkyne Cycloadditions. Science. 2013; 340(6131):457. [PubMed: 23558174]

55. Rodionov VO, Fokin VV, Finn MG. Mechanism of the Ligand-Free CuI-Catalyzed Azide – Alkyne Cycloaddition Reaction. Angew Chem Int Ed. 2005; 117(15):2250.

56. Snyder RG, Strauss HL, Elliger CA. C-H Stretching Modes and the Structure of n-Alkyl Chains 1: Long, Disordered Chains. J Phys Chem. 1982; 86(26):5145.

57. Paoprasert P, Spalenka JW, Peterson DL, Ruther RE, Hamers RJ, Evans PG, Gopalan P. Grafting of poly(3-hexylthiophene) brushes on oxides using click chemistry. J Mater Chem. 2010; 20(13): 2651.

58. Sahoo RR, Patnaik A. Binding of fullerene C-60 to gold surface functionalized by self-assembled monolayers of 8-amino-1-octane thiol: a structure elucidation. J Colloid Interface Sci. 2003; 268(1):43. [PubMed: 14611770]

59. Hamwi A, Latouche C, Marchand V, Dupuis J, Benoit R. Perfluorofullerenes: Characterization and structural aspects. J Phys Chem Solids. 1996; 57(6–8):991.

60. Lin Z, Strother T, Cai W, Cao XP, Smith LM, Hamers RJ. DNA attachment and hybridization at the silicon (100) surface. Langmuir. 2002; 18(3):788.

61. Olsson COA, Hörnström SE. An AES and XPS study of the high alloy austenitic stainless steel 254 SMO® tested in a ferric chloride solution. Corros Sci. 1994; 36(1):141.

62. Devadoss A, Chidsey CED. Azide-Modified Graphitic Surfaces for Covalent Attachment of Alkyne-Terminated Molecules by "Click" Chemistry. J Am Chem Soc. 2007; 129(17):5370. [PubMed: 17425323]

63. Gouget-Laemmel AC, Yang J, Lodhi MA, Siriwardena A, Aureau D, Boukherroub R, Chazalviel JN, Ozanam F, Szunerits S. Functionalization of Azide-Terminated Silicon Surfaces with Glycans Using Click Chemistry: XPS and FTIR Study. J Phys Chem C. 2013; 117(1):368.

64. Baltrusaitis J, Jayaweera PM, Grassian VH. XPS study of nitrogen dioxide adsorption on metal oxide particle surfaces under different environmental conditions. Phys Chem Chem Phys. 2009; 11(37):8295. [PubMed: 19756286]

Highlights

- We investigate the formation of high-coverage monolayers of nanoparticles.
- We use “click chemistry” to form these monolayers.
- We form multiple layers based on the same strategy.
- We confirm the formation of covalent bonds spectroscopically for up to 3 layers.
- We confirm that chemical attachment, not self-assembly, drives the process.

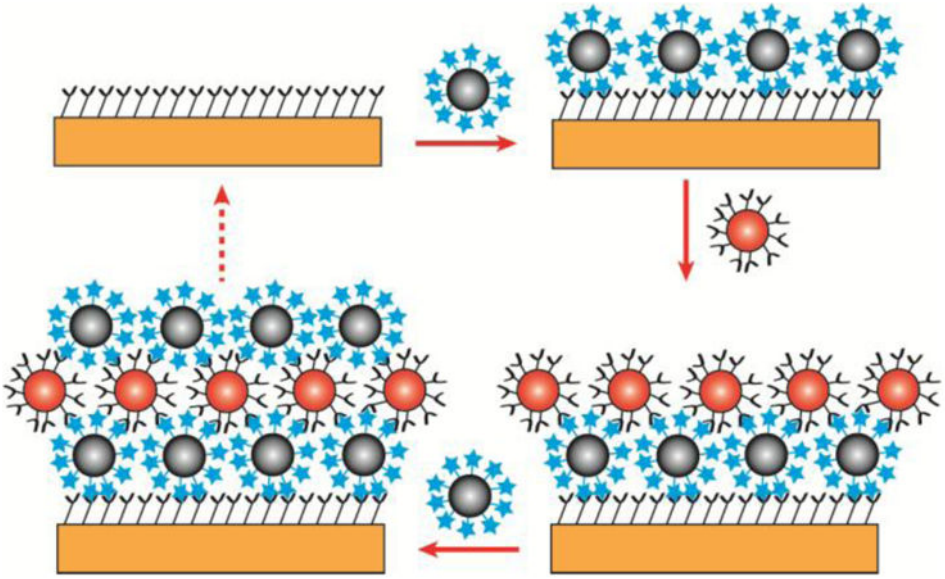

Figure 1.

Basic scheme of nanoparticle layer deposition. After modifying the surface with azide functionality, a layer of complementary alkyne functionalized nanoparticles is deposited on the surface. This surface is now the basis for the second layer of nanoparticle deposition. Each layer can be used as a starting point for the complementary functionalized layer.

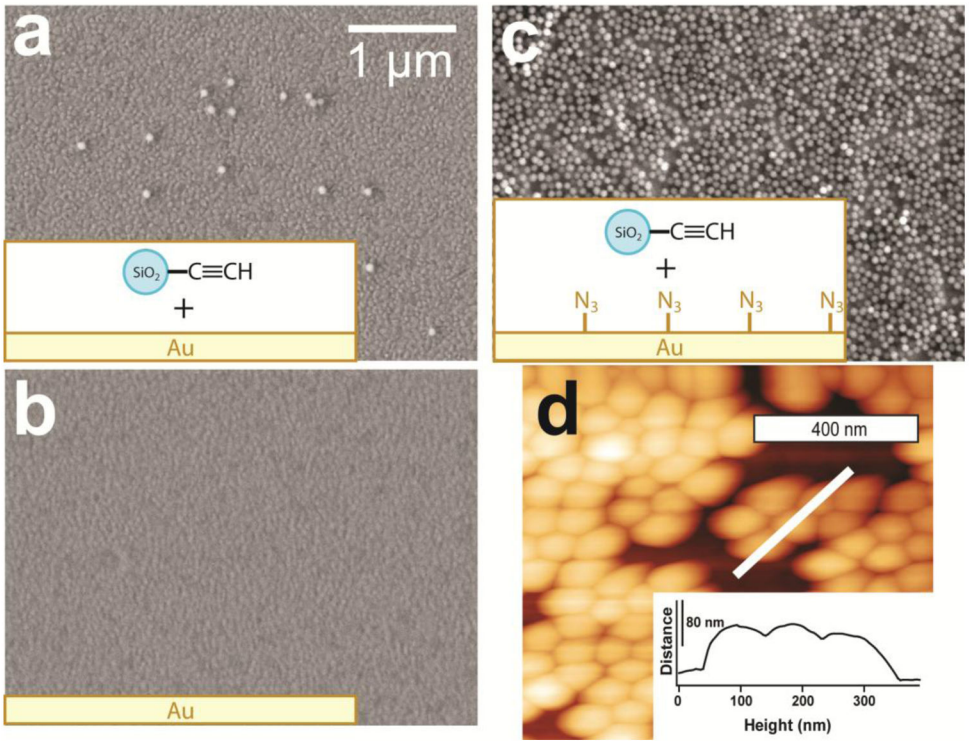

Figure 2.

Control experiments to show the importance of the complimentary chemistry and the stable nature of the triazole ring. The figure shows (a) the procedure for the first layer nanoparticle deposition as described in the text sans for azide termination of the gold substrate and washing; (b) the same procedure for first layer nanoparticle deposition sans for azide termination of the gold substrate (but washed and sonicated in methanol); and (c) the procedure as written (for reference, with all steps included). Part (d) shows an AFM image of a single layer of nanoparticles of 80 nm in diameter attached by “click chemistry” to the same substrate.

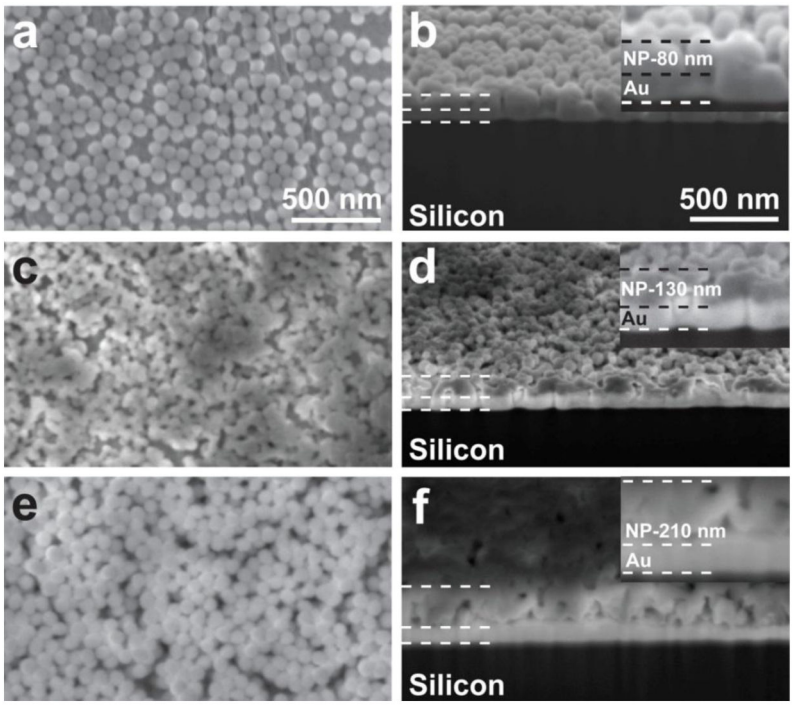

Figure 3.

SEM studies to determine the surface coverage and film thickness. The figure shows: (a) the 80 nm alkyne nanoparticle-deposited layer surface (plan view); (b) the cross sectional view of the 80 nm alkyne nanoparticle layer; (c) the 50 nm azide nanoparticle-layer surface (plan view) deposited on top of the first layer; (d) the cross sectional view of 50 nm azide nanoparticles layer deposited on top of the first layer; (e) the second 80 nm alkyne nanoparticle-deposited layer surface (third overall layer, plan view); and (f) the second cross sectional view of the three-layer system.

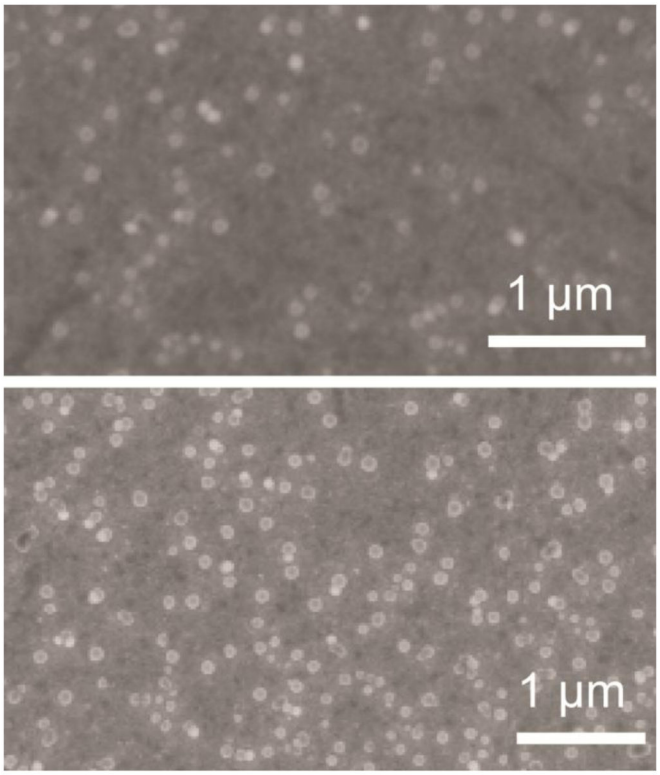

Figure 4.

SEM study of low (top) and higher (bottom) coverage 80 nm alkyne-functionalized SiO_2 nanoparticles attached to the azide-terminated surface. The process of covalent attachment is random, confirming that self-assembly is not the driving force behind the monolayer formation.

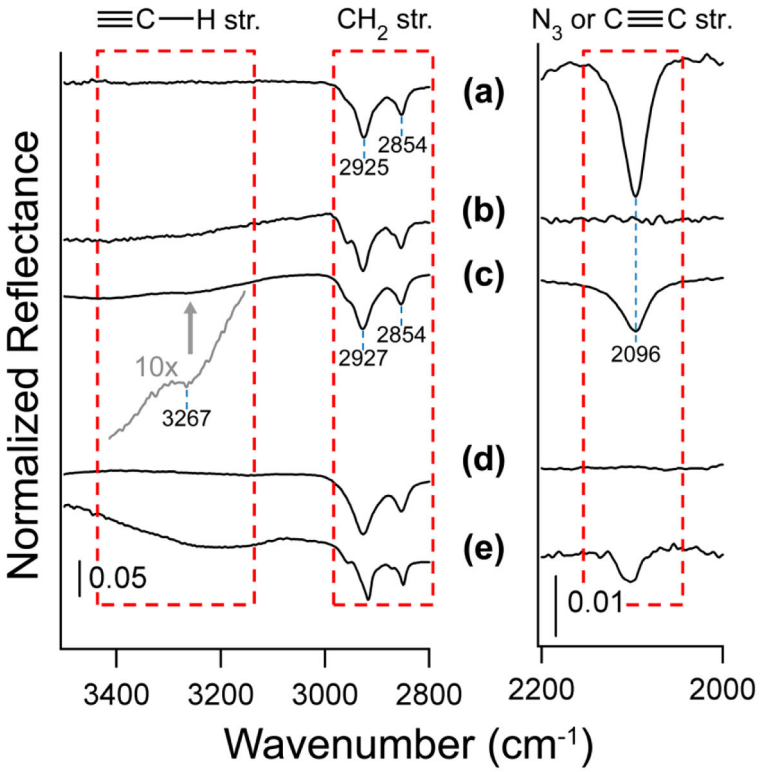

Figure 5.

Infrared spectroscopy investigation of NPLD following deposition of each nanoparticle layer. ATR FT-IR spectra of (a) 11-azido-undecanethiol modified Au substrate; (b) azide-modified substrate (a) following reaction with 5-hexynoic acid; (c) 80-nm alkyne functionalized nanoparticles deposited onto sample (a); (d) first-layer sample (c) following reaction with 5-hexynoic acid; and (e) 50-nm azide functionalized nanoparticles deposited on sample (c). The gray line shows the alkyne C-H stretch of spectrum (c) magnified 10 times.

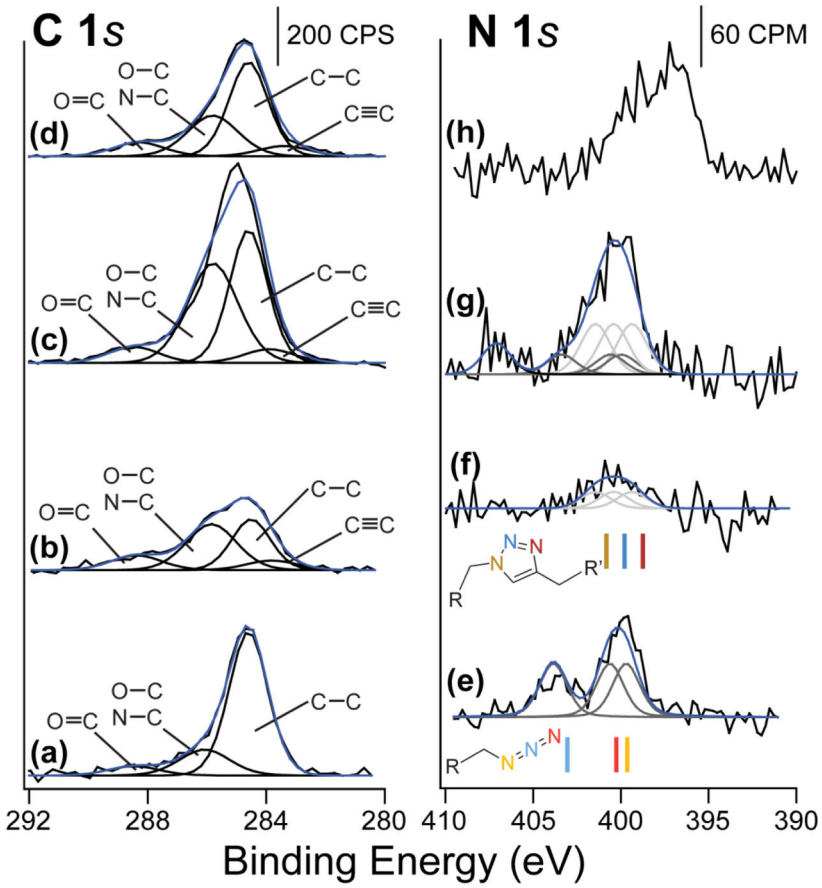

Figure 6.

XPS investigation of NPLD following deposition of each nanoparticle layer. On the left is the C 1*s* region, and the right panel shows the N 1*s* region of: (a,e) the azide-terminated gold surface; (b,f) the alkyne-terminated 80-nm nanoparticle deposited onto azide-terminated gold surface; (c,g) the azide-terminated 50-nm nanoparticles deposited onto the first 80-nm nanoparticle layer; and (d,h) the second 80-nm alkyne-terminated nanoparticle layer on the 50-nm azide nanoparticle layer. The solid lines in the N 1*s* region below the experimental spectra show the predicted energy shifts from DFT calculations. The colors of each bar correspond to the colors of the nitrogen atoms in the model, and the lighter lines show the azide information while the darker lines provide information for the triazole ring compound. It is expected that a mixture of species is observed beyond the first layer.